ACS APPLIED MATERIALS & INTERFACES

www.acsami.org

Research Article

Self-Folding Liquid Crystal Network Filaments Patterned with Vertically Aligned Mesogens

Dae Seok Kim, Young-Joo Lee, Yuchen Wang, Jinseok Park, Karen I. Winey, and Shu Yang*

Cite This: *ACS Appl. Mater. Interfaces* 2022, 14, 50171−50179

Read Online

ACCESS | Metrics & More | Article Recommendations | Supporting Information

ABSTRACT: Fibrous soft actuators with high molecular anisotropy are of interest for shape morphing from 1D to 2D and 3D in response to external stimuli with high actuation efficiency. Nevertheless, few have fabricated fibrous actuators with controlled molecular orientations and stiffness. Here, we fabricate filaments from liquid crystal networks (LCNs) with segmental crosslinking density and gradient porosity from a mixture of di-acrylate mesogenic monomers and small-molecule nematic or smectic liquid crystals (LCs) filled in a capillary. During photopolymerization, phase separation between the small-molecule LCs and LCN occurs, making one side of the filament considerably denser than the other side. To direct its folding mode (bending or twisting), we control the alignment of LC molecules within the capillary, either along or perpendicular to the filament long axis. We show that the direction of UV exposure can determine the direction of phase separation, which in turn direct the deformation of the filament after removal of the small-molecule LCs. We find that the vertical alignment of LCs within the filament is essential to efficiently direct bending deformation. By photopatterning the filament with segmental crosslinking density, we can induce a reversible folding/unfolding into 2D and 3D geometries triggered by deswelling/swelling in an organic solvent. Moreover, by taking advantage of the large elastic modulus of LCNs and large contrast of the modulus before and after swelling, we show that the self-folded LCP filament could act as a strong gripper.

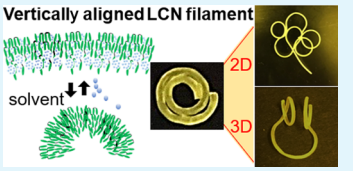

KEYWORDS: *liquid crystal network filament, self-folding, soft actuator, molecular alignment, photo-patterning*

1. INTRODUCTION

Shape morphing of soft materials in response to external stimuli has attracted tremendous attention for potential applications, including sensors,[1] drug delivery systems,[2] energy generators,[3] actuators,[4] artificial muscles,[5] soft robotics,[6] and smart fabrics.[7] To fold materials from one- (1D) or two-dimensional (2D) to three-dimensional (3D) structures, the materials will undergo different types of elastic deformation, including bending, twisting, and curling. Thus, the ability to program the deformation modes on demand will enable creation of complex 3D structures with new functions.[8,9] In principle, folding can be achieved when there is a differentiated volume change and/or variation of elastic moduli, e.g., in a bilayer structure.[10] Accordingly, a wide range of stimuli-responsive soft materials, such as hydrogels,[11] shape memory polymers,[12] liquid crystal polymers (LCPs)[13] including glassy liquid crystal networks (LCNs) and liquid crystal elastomers (LCEs), dielectric elastomers,[14] and pneumatically actuated elastomers,[15] have been investigated to realize the 3D complex folding, triggered by solvent, heat, light, magnetic field, electric field, or pressure. Among them, LCEs and LCNs that have intrinsic anisotropy are attractive because their shape changes can be preprogrammed over multiple length scales by aligning LC mesogens in the networks in certain orientations. LCEs that are loosely crosslinked contract along the parallel direction and expand in the perpendicular direction of the director field when the mesogens undergo a thermal transition from the nematic to the isotropic phase.[16] In contrast, LCNs that are more densely crosslinked usually present no thermal transition from nematic to isotropic phases, thus rarely responding to heat.[13] However, LCNs can contract and expand in the direction perpendicular to the director field upon swelling and deswelling by a solvent or chemical.[17,18] LCEs typically have elastic modulus $E \sim 0.1-5$ MPa and glass transition temperature (T_g) below 0 °C, where the highly crosslinked LCNs have $E \sim 0.8-2$ GPa and $T_g \sim 40-120$ °C.[13] On the other hand, the high elastic moduli are advantageous when fast speed[19] and large load bearing capability[20] are desired.

Compared with 2D films or 3D bulk geometries such as spheres, filaments offer greater degrees of freedom for realizing complex shapes at a faster speed.[21] When they are connected or bundled together properly, they could offer higher efficiency and strength as shown in spider silks and artificial muscles.[22,23] Recently, LCN and LCE fibers and filament actuators have been fabricated for applications, including artificial muscles,[24] smart textiles,[25] optical waveguides,[26] cargo robots,[27] fluidic vessel,[28] and optical pliers.[29] Most of them are fabricated by

Received: August 19, 2022
Accepted: October 13, 2022
Published: October 25, 2022

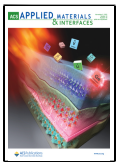

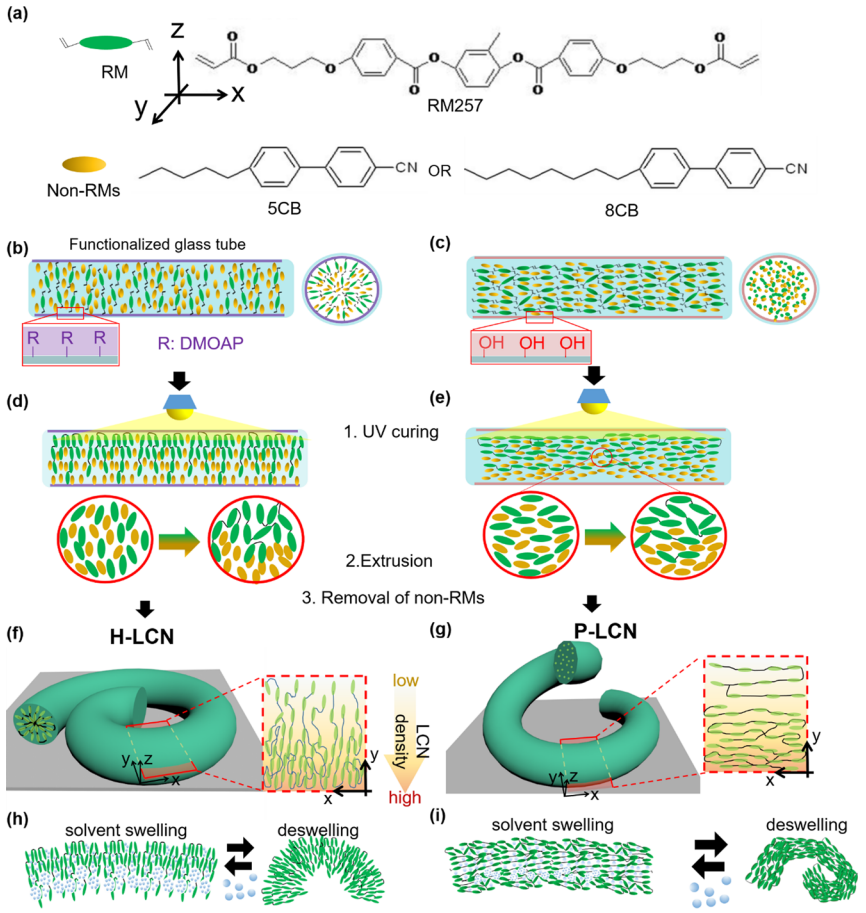

Figure 1. Illustrations of the steps for fabrication of LCN filaments with different surface anchorings. (a) Molecular structures of the reactive mesogenic monomer, RM257, and nonreactive mesogens (non-RM), 5CB and 8CB, respectively. (b,c) Illustration of the orientation of RM mixtures infiltrated into chemically functionalized glass capillary tubes with planar and homeotropic anchoring. (b,d,f) Fabrication process of the homeotropic anchoring LCN (H-LCN) filament and 3D sketch of H-LCN folding after removal of non-RMs. (c,e,g) Fabrication process of the planar anchoring LCN (P-LCN) filament and 3D sketch of P-LCN folding after removal of non-RMs. Insets of (d,e) illustrate phase separation of nonreactive LCs from RMs during UV polymerization. (h,i) Illustrations of the actuation of H-LCN and P-LCN filaments by solvent swelling and deswelling, respectively.

shearing-based techniques such as 3D printing,[30] electrospinning,[31,32] microfluidics,[33] and their combination,[34] where the mesogens are aligned in parallel to the liquid flow direction. In 2D films, folding is typically achieved via bending at the creases due to the mismatch of density or moduli in multilayer structures[35,36] or splay alignment of mesogens.[37] In contrast, fibrous geometries have shown rich geometric couplings between twist and bend deformations due to their slender geometries.[38] For example, a gradient in mass density,[39] tensile moduli,[40,41] or nonuniaxial molecular orientation along the fiber diameter[42−44] has led to the formation of complex coiled and plectonemic structures due to an occurrence of disorderly torsional deformation as frequently seen in nature,[45,46] which are fascinating but extremely challenging to uniaxially deform in 3D; thus, unwanted deformation of twisting or entanglement is unavoidable. Therefore, in the fibrous structures, the orientation control of the polymeric chain seems to be more important for the uniaxial deformation than 2D and 3D bulk structures. It has been suggested[47,48] that the efficiency of folding in a polymeric material with a density gradient in response to chemical stimuli can be maximized when the folding direction and their chain orientation are perpendicular to each other. Nevertheless, in the production of filaments or fibers using LC monomers, control of the orientation of polymer chains perpendicular to the director field, referred as homeotropic anchoring, has not been demonstrated. To better direct the LC alignment inside a filament geometry, LC mesogens should have large surface anchoring strength so that they can follow the orientation imposed by surface alignment. Previously, we and others[49−51] have shown that LC monomer anchoring strength can be enhanced by addition of nonreactive small-molecule mesogens, which also lowers the viscosity for infiltration in an LC cell. Furthermore, the mixtures of reactive and nonreactive mesogens have been used to form anisotropic porous structures due to phase separation of small-molecule LCs from the polymerized networks.[52,53] Here, by taking advantage of the phase separation during photopolymerization and surface alignment techniques, we fabricate a self-folding LCN filament with vertical alignment of mesogens in the smectic A (SmA) LC phase, possessing a quasi-long-range positional order in the direction normal to the layers. In comparison with LCN filaments with parallel mesogen alignment, those with the vertical alignment exhibit better controllability in 3D folding, which can be triggered reversibly by solvent swelling and deswelling. The extent of the folding can be fine-tuned by the intensity and exposure direction of the UV light during photopolymerization, allowing us to create segmental cross-

https://doi.org/10.1021/acsami.2c14947
ACS Appl. Mater. Interfaces 2022, 14, 50171−50179

linking density within the filaments to program the folded shapes. Moreover, LCNs are glassy in the dry state with $E \sim$ 650 MPa but become soft and rubbery with $E \sim 1$ MPa upon swelling by a solvent. The swollen LCN filament can conform over an object and then self-fold into a dumbbell shape to grab the object during drying. The rigid folded filament can hold a weight up to ∼7000 times its own weight.

2. METHODS

2.1. Materials. 1,4-Bis-[4-(6-acryloyloxypropyloxy)benzoyloxy]-2-methylbenzene (RM257), 4-cyano-4-pentylbiphenyl (5CB), and 4-cyano-4-octylbiphenyl (8CB) were purchased from Tokyo Chemical Industry (TCI) Co. (Figure 1a). *N*,*N*-Dimethyl-*n*-octadecyl-3-aminopropyltrimethoxysilyl chloride (DMOAP), chloroform, methylene chloride (DCM), and ethanol were purchased from Sigma Aldrich. A photoinitiator, Irgacure 369, was purchased from Ciba. Poly(vinyl alcohol) (PVA, molecular weight 9k−10k) was purchased from Sigma-Aldrich. All chemicals were used as received. A glass capillary tube was purchased from World Precision Instruments (WPI).

2.2. Surface Modification of the Glass Capillary Tubes. To create a planar anchoring surface, the capillary tubes were immersed in the piranha solution, which is a mixture of sulfuric acid and 30% hydrogen peroxide solution (3:1 v/v), for 1 h at 70 °C to generate hydroxyl groups, followed by washing with deionized (DI) water three times. Then, the inside of the glass capillary tube was coated with a thin layer (a few nanometers) of PVA to guide planar anchoring by infiltrating an aqueous solution of 1 wt % PVA, followed by air drying.

To create a homeotropic anchoring surface, the glass capillary tubes were immersed in 3 vol % DMOAP solution (water/ethanol, 1:9 v/v) for 30 min, followed by rinsing with DI water three times and baking at 110 °C in a convection oven for 1 h.

2.3. Preparation of LCNs. The photopolymerizable LC mixtures are prepared by mixing RM257 with 5CB or 8CB of different mass concentrations and 2 wt % Irgacure 369 with respect to the mass of RM257. To get a homogeneous mixture, all components are first dissolved in excess DCM, followed by evaporation under stirring at 40 °C overnight and at 30 °C for another 2 h. The LCN filaments were prepared by capillary infiltration of the mixtures into surface-treated glass capillaries, followed by photopolymerization under 365 nm UV light (Newport Hg 97435 Oriel Flood Exposure Source) though a photomask at the same total dosage of 8.0 J/cm^2 with variable intensities. Then, a gastight glass syringe (Hamilton Company, U.S.) with a 21G-needle was used to manually push out the LCN filament by applying a pneumatic pressure (∼10^4 kPa) inside the glass capillary. The filaments were then washed with ethanol to remove nonreacted 5CB, 8CB, or RM257.

2.4. Characterization. Alignments of LCN filaments were characterized using an Olympus BX61 motorized optical microscope with crossed polarizers using CellSens software. Scanning electron microscopy (SEM) was performed using an FEI Quanta 600 ESEM at 5KV. All digital images were taken by iPhone 6 Pro. X-ray scattering experiments were performed on the Dual-source and Environmental X-ray Scattering (DEXS) facility at the University of Pennsylvania. A Xeuss 2.0 with a GeniX3D S4 source (Cu Kα, λ = 1.54 Å) and a PILATUS3 1M detector (981 × 1043 pixels, pixel dimension 172 μm) was used with a sample-to-detector distance of 16 cm. The HLCN and PLCN samples are measured in a transmission configuration where the long axis of the filament is placed horizontally relative to the 2D detector. The tensile tests were performed using an Instron 5564 model, with a tensile load cell of 10 N. The speed of the moving load cell was fixed at 2 mm min^{-1}. Fourier transform infrared (FT-IR) spectra were obtained from Nicolet Nexus 470 using potassium bromide (KBr) pellets with a resolution of 4 cm^{-1}. Before being pelleted, samples were washed with ethanol to remove non-RMs and dried in a vacuum oven at 40 °C. Differential scanning calorimetry (DSC) tests were performed with a TA Instruments Q2000 using an aluminum hermetic crucible. Samples were heated and cooled at a ramping rate of 10 °C/min for two cycles, and data from the 2nd cycle were reported here.

3. RESULTS AND DISCUSSION

In order to generate the uniaxially folding filament, we design a LCN filament to have a density gradient along the diameter and controlled alignment where the mesogens are oriented normal to the surface of the filament, referred to as the H-LCN filament. The self-folding actuation of the H-LCN is investigated, triggered by solvent swelling and deswelling processes. Moreover, in the experiment, we compare the folding behavior of the H-LCN filament by comparing with a LCN filament with planar alignment where the mesogens are aligned along the long axis of the filament, referred to as the P-LCN filament. The LCN filaments are fabricated by infiltrating a mixture of nonreactive mesogens (non-RM), including 4-cyano-4-pentylbiphenyl (5CB) for the nematic phase and 4-cyano-4-octylbiphenyl (8CB) for the SmA phase, and reactive mesogenic monomers (RMs), 1,4-di(4-(3-acryloyloxypropyloxy)benzoyloxy)-2-methylbenzene (RM257), into a glass capillary tube (diameter, ∼800 μm) with homeotropic (i.e., molecular directors of LC mesogens are perpendicular to the surface) or planar anchoring conditions, followed by photopolymerization (Figure 1b−e). Since the shearing force generated by capillary infiltration of the monomer mixtures is very small compared with extrusion techniques such as 3D printing under an external pressure, the alignment of RMs within the capillary is critically dependent on the surface anchoring of the mixture, which is mainly governed by the competition between surface anchoring energy and elastic energy of LCs. Here, introduction of the non-RM (5CB or 8CB), which have much larger surface anchoring energy than RMs and act as mesogenic diluents as they have lower viscosity than RMs, enables success to guide the RM orientation within the capillary.[54] For planar anchoring, the capillary tubes were coated with PVA and rubbed with a velvet yarn along the long axis of the tube. For homeotropic anchoring, the cleaned capillary tube was silanized with dimethyloctadecyl[3-(trimethoxysilyl)propyl]-ammonium chloride (DMOAP), where the extended long alkyl chains induce an intercalation with rodlike LC molecules, here 8CB or 5CB (Figure 1b,c).[55,56] The RM mixture was then infiltrated into the capillary tube through capillary action, followed by photopolymerization under UV light with variable intensities to control the density gradient through the filament thickness. Since the capillary tube had a rather larger diameter, ∼800 μm, the mixture was in the nematic or smectic A phase with birefringence, thus seeing limited penetration of UV light through the capillary tube.[37] Since polymerization occurred mostly at the top of the filament surface, a crosslinking density gradient along the diameter of the LCN filament was observed (Figure 1d,e). Meanwhile, the initially miscible RM mixture became phase separated as polymerization proceeded, where non-RMs were excluded from the polymer network, referred to as poly(RM257), which further limited the light penetration inside the tube. Since the direction of UV exposure to the capillary determines the direction of the density gradient in the LCN filament, initially the homogeneous state of the mixture between RM257 and 8CB or 5CB should be retained to avoid any phase separation before the polymerization process. In order to estimate the miscibility between RM257 and 8CB, DSC analysis was conducted (Figure S1), showing characteristic of a single LC material with peaks representing phase transition temperatures, which are not appeared in pure RM257 and 8CB. We further attempted to directly observe the

https://doi.org/10.1021/acsami.2c14947
ACS Appl. Mater. Interfaces 2022, 14, 50171−50179

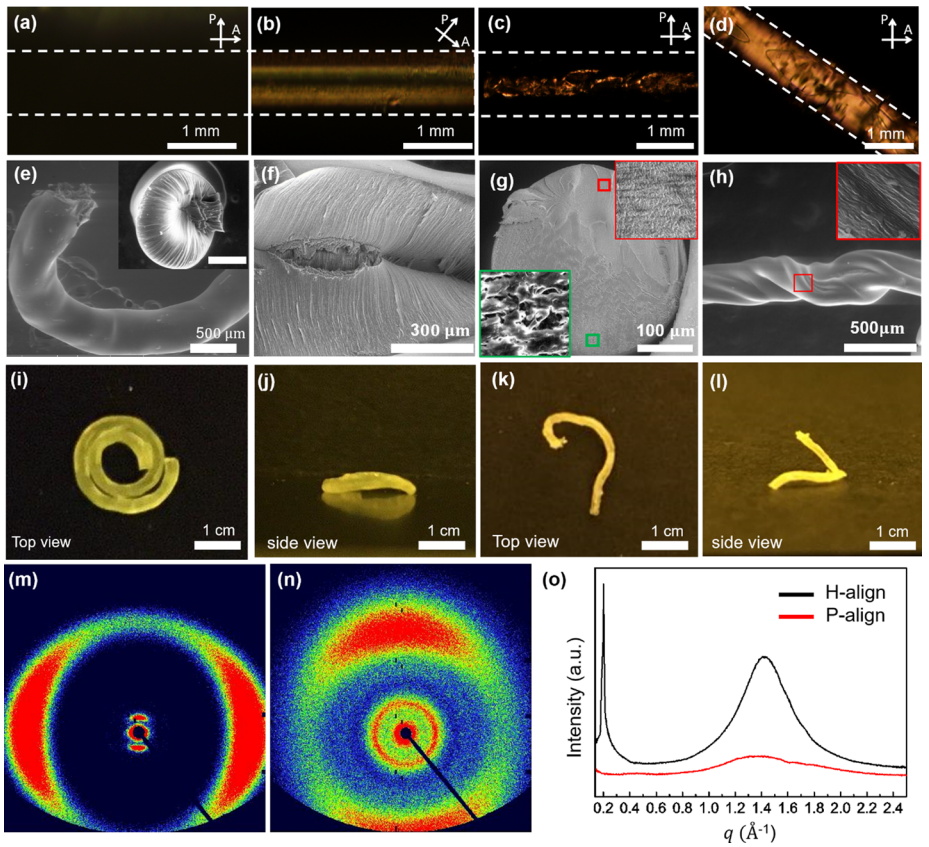

Figure 2. Characterization of H-LCN and P-LCN filaments. (a–d) POM images of (a,b) H-LCN and (c,d) P-LCN, where the cross polarizers are (a) 90° and 45° relative to each other. (e–h) SEM images of H-LCN and P-LCN filaments. The inset of (e) shows the cross-sectional view of H-LCN. Scale bar: 200 μm. Lateral cross-section of H-LCN showing vertical alignment along the filament, shown in (f). (g) Cross-sectional view of P-LCN showing the density gradient along the thickness from the UV directly exposed side (red box) to the opposite sides (green box). (h) P-LCN filament shows twisted form, while the inset of (h) shows the alignment parallel to the filament (red box). (i–l) Photographs of (i,j) H-LCN and (k,l) P-LCN filaments viewed from the top and the side, respectively. (m,n) X-ray scattering patterns of (m) H-LCN and (n) P-LCN filaments, respectively. The circle pattern in (n) is from the Kapton background. (o) 1D profile of the azimuthally integrated 2D patterns of H-LCN and P-LCN filaments.

solubility between 8CB or 5CB with different mass loadings of RM257 (20, 40, 60, and 80 wt %), which all appeared homogeneous (Figure S2), in agreement with literature studies based on DSC data.[57−59] However, when the mixture dwelled at room temperature for 2−3 days (~54 h), phase separation occurred (Figure S3), and the RM257 layer did not clear up even at ~200 °C, suggesting that they were crosslinked. This is because diacrylate monomers can undergo free-radical polymerization by light and/or heat, although the latter is much slower.[60] Thus, we fabricated the LCN filament as soon as the mixture was prepared in order to minimize other factors to influence the polymerization before UV curing.

As a result, non-RMs were pushed downward to the bottom of the tube, where therefore was less polymerized (Figure 1d,e). After the LCN filament was extruded out of the glass tube, the non-RMs and RMs that were not crosslinked were removed by washing with ethanol, followed by drying, leading to bending or twisting due to preferential shrinkage in the direction that is along or perpendicular to the mesogen orientation (Figure 1f,g). The gel fraction of the LCN is estimated to be ~86% by comparing the weight before and after washing with ethanol. The LCN filaments could recover the shape when immersed in an organic solvent, chloroform, which has a relatively high solubility parameter for poly-(RM257),[52] illustrating a reversible folding actuation triggered by swelling and deswelling (Figure 1h,i). Compared to the P-LCN filament, where the polymer network can undergo both lateral and out-of-plane contraction such that bending and twisting occur at the same time without much control of each (Figure 1g,i), the H-LCN filament bends only (Figure 1f,h). To create the H-LCN filament, RM257 was mixed with 8CB in its smectic phase at room temperature and infiltrated into a DMOAP-treated capillary tube. Here, 8CB was only allowed to have splay elastic deformation not bending and twisting deformation in the molecular ordering.[61]

Figure 2a,b shows the polarized optical microscopy (POM) images of H-LCN filaments with 14 wt % RM257. Figure 2a shows extinction of birefringence between the two crossed polarizers at 90°, while Figure 2b with two cross polarizers at 45° shows a bright color with the extinction line appeared at the center of the filament, which is the dislocation line along the long axis of the filament. After removal of 8CB, the vertical alignment of poly(RM257) can be clearly seen in SEM images (see the inset of Figure 2e,f). Since the homeotropic anchoring is guided by 8CB at room temperature, while RM257 is in the nematic phase up to 70 to 126 °C, depending on the concentration of RM257, the smectic ordering of the mixture could be destroyed as the concentration of RM257 increases. Indeed, when RM257 in the mixture was increased to above 18 wt %, the smectic phase was lost as confirmed by DSC (Figure

https://doi.org/10.1021/acsami.2c14947
ACS Appl. Mater. Interfaces 2022, 14, 50171−50179

S1). An escaped configuration of the LCN mixture with 18 wt % RM257 in the DMOAP-coated glass capillary was confirmed by POM and SEM (Figure 3a–d), where the director field is

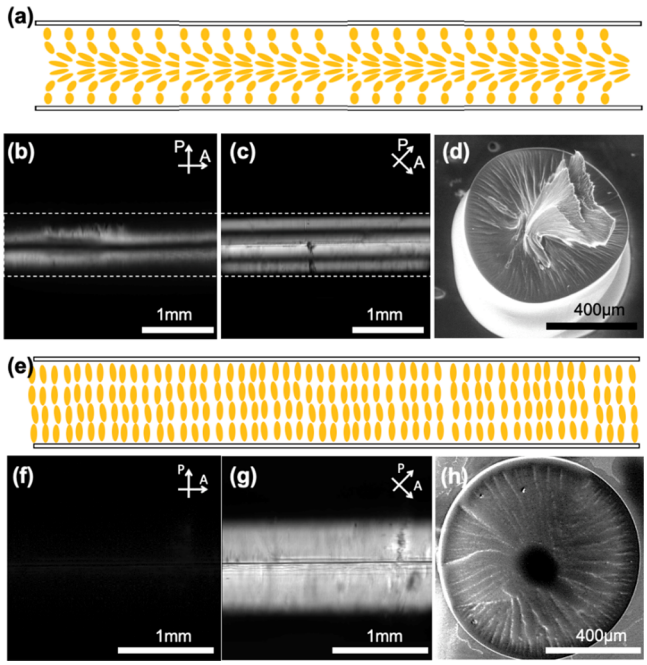

Figure 3. P-LCN filament with escaped and radial configurations of the director field. (a) Schematic of the escaped director field confined in a cylinder. (b,c) POM images of the escaped P-LCN filament with the analyzer parallel and 45°-rotated with respect to polarizer, respectively. (d) Cross-sectional SEM image of the escaped P-LCN filament. (e) Schematic of the radial director field confined in a cylinder. (f,g) POM images of the radial H-LCN filament with the analyzer parallel and 45°-rotated with respect to the polarizer, respectively. (h) Cross-sectional SEM image of the radial-oriented H-LCN filament.

conically bent at the core of the filament, characteristic of the nematic phase in the cylindrical confinement to avoid elastic penalty caused by the line defect in the core.[62] The smectic ordering of poly(RM257) with 8CB started to emerge below ~17.3 wt % RM257, presenting a radial configuration along the long axis of the glass capillary (Figure 3e–h). In comparison, the P-LCN filament has more complex disclination lines along the filament where the polymer chains deviate from the principal axis (Figure 2c,d). Since the ordering range of the nematic LCs is typically up to hundreds of microns (~10^5 molecular lengths),[63] the disclination lines are inevitably formed throughout the filament that is centimeters long.

After photopolymerization of the RM mixture and removal of non-RMs, both types of filaments showed bending (Figure 2i–l) due to asymmetric density distribution of poly(RM257) within the filament, as shown in the cross-sectional SEM images (Figures 2g and S4). As expected, the P-LCN filament showed not only bending but also twisted distortion (Figure 2h,k,l), whereas the H-LCN filament showed only bending deformation (Figure 2e,i,j).

To investigate the internal organization of the poly(RM257) filaments at the molecular level, X-ray scattering experiments were carried out (see Figure 2m–o) across a wide angular range, where the X-ray beam was perpendicular to the filaments and the filaments are arranged horizontally relative to the 2D detector. In the 1D plots of the circularly averaged intensity (Figure 2o), a broad peak at the scattering vector, $q \sim 1.53$ Å^{-1}, is observed, corresponding to a plane spacing of 4.1 Å, in agreement with a typical value of π–π stacking distance between the mesogens in poly(RM257). The scattering 2D patterns show that the π–π stacking peak appears in the perpendicular (for the H-LCN filament) and parallel (for the P-LCN filament) directions to the long axis of each filament, respectively, confirming their molecular alignment within the filaments (Figure 2m,n). In the case of the H-LCN filament, a lower-angle peak at $q \sim 0.222$ Å^{-1} (or ~27.7 Å) corresponds to the length of a RM257 monomer, ~25.6 Å.[52] The result indicates that poly(RM257) has a smectic A layering arrangement in the H-LCN filament, though it was difficult to observe in cross-sectional SEM (Figure 2f). Clearly, the smectic LC, 8CB, plays a crucial role in inducing smectic A layering arrangement of RM257 in the capillary tube. It is also noted that the absolute circularly averaged intensity is higher in H-LCN than that of P-LCN filaments (Figure 2o), attributed to the formation of a higher ordered smectic phase along the radius, ~400 μm shrunk from the 800 μm tube diameter, in contrast to the nematic phase in the P-LCN filament along the long axis of the filament, which is a few centimeters long.

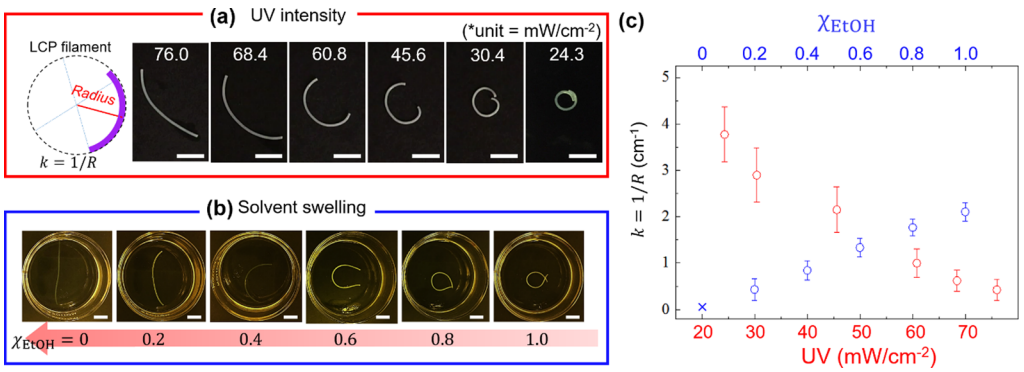

Figure 4. Controlled bending of the H-LCN filaments by variable UV intensities and solvent compositions. (a) Photographs of H-LCN filaments cured at different UV intensities, showing higher curvatures as the UV intensity decreases. The overall dosage for each filament was kept the same at 8.0 J/cm^2. (b) Photographs of H-LCN filaments cured at 24.3 mW/cm^{-2} in mixed solvents of ethanol and chloroform of different volume fractions of ethanol. (c) Phase diagram of the curvatures of the bent filaments as a function of UV intensities (red circles) and volume fractions of ethanol (blue circles). All scale bars are 1 cm.

https://doi.org/10.1021/acsami.2c14947
ACS Appl. Mater. Interfaces 2022, 14, 50171–50179

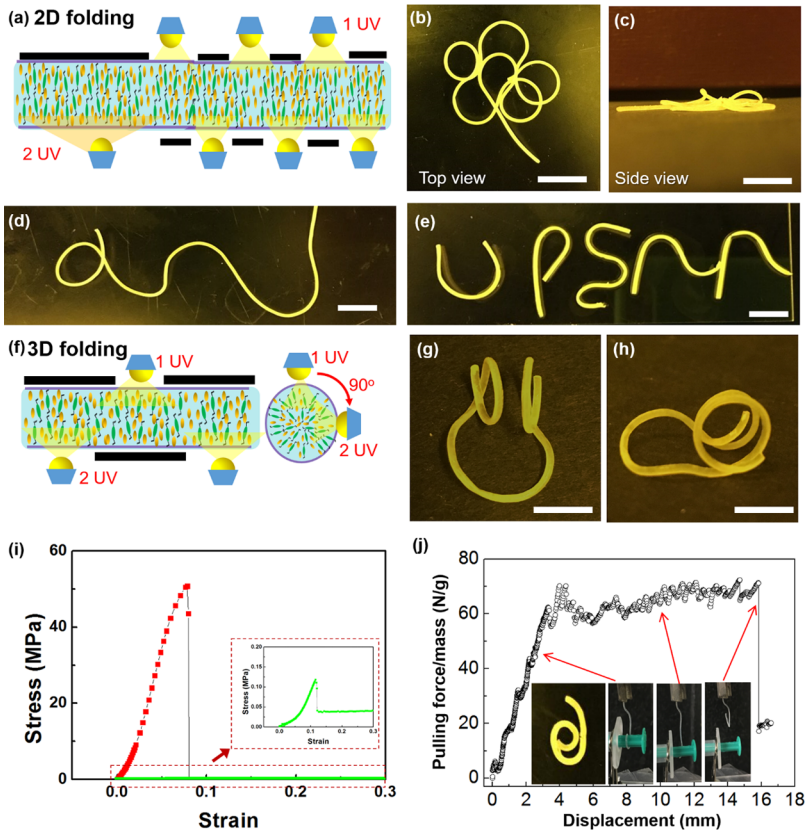

Figure 5. Patterning of H-LCN filaments and their mechanical properties. (a) Illustrations of preparation of 2D of H-LCN filaments. UV-1 refers to the first UV exposure, and UV-2 refers to the second UV exposure. (b,c) Photographs of the flowerlike objects folded from H-LCN in top and side views, respectively. The scale bars are 1 cm. (d) Various curvatures generated from a single H-LCN filament. The scale bar is 1 cm. (e) Demonstration of letters "UPENN" where each fiber has its own curvature. The scale bar is 1 cm. (f) Illustrations of preparation of 3D of H-LCN filaments. Sequentially, the sample is first UV exposed (UV-1) and rotated by 90° and then the second UV exposed (UV-2). (g,h) Photographs of 3D folded H-LCN filaments from top and side views, respectively. All scale bars are 1 cm. (i) Strain−stress curves of H-LCN in the dried state (red dots) and a solvent swollen (green dots) state. (j) Pull force of the H-LCN gripper from caging the cylindrical object to its separation. Inset: Photos at each step.

We then explore control of the polymer crosslinking density gradient along the filament thickness to fine tune the extent of bending (Figure 4a). In Figure 4a, different H-LCN filaments were prepared with the same amount of RM257/8CB mixture (14 wt % of RM257) at varying UV intensities, 76, 68.4, 60.8, 45.6, 30.4, and 24.3 mW/cm^{-2}, respectively, at the same total dosage, 8.0 J/cm^2. At the lower UV intensity, fewer radicals are generated, leading to higher crosslinking densities in the regions closer to the UV light.[52,64] In FT-IR spectra, poly(RM257) shows two distinct peaks at 810 and 1750 cm^{-1}, corresponding to the out-of-plane vibration of the C−H bond of the acrylate group and the C═O stretching vibration of the mesogenic acrylate ester group, respectively (Figure S5).[65] As the di-acrylate groups in RM257 are polymerized, the peak at 810 cm^{-1} decreases with the increase of UV intensity, and the peak at 1750 cm^{-1} was independent of photopolymerization intensity and therefore was used to normalize the spectra. We found that the conversion of RM257 monomers to poly(RM257) was comparable regardless of UV intensities since the total dosage was the same. Therefore, the crosslinking density distribution along the diameter was only varied by UV intensities not by the total amount of the crosslinking density. In turn, the filament should bend away from the low crosslinking side, which swells more. Supporting this, we tested the swelling behaviors using mixed solvents of ethanol and chloroform, which are a bad solvent and a good solvent for poly(RM257), respectively (Movie S1).[52] Figure 4b shows the swelling behaviors of H-LCN filaments (UV intensity = 24.3 mW/cm^{-2}) dipped in ethanol/chloroform mixed solvents of different volume fractions of ethanol ($x_{ethanol}$). As seen in Figure 4c, the curvature of H-LCN filaments ($k = 1/R$) decreases with the increase of the UV intensity and the bent filament in the dry state had $k \sim 3.8$ cm^{-1}, which gradually decreases as $x_{ethanol}$ decreases.

Encouraged by these results, we investigated how to control both the direction and degree of bending of H-LCN filaments by selective UV irradiation at specified locations within the capillary tube. For example, to induce 2D-patterned folding of the filament, a three-step photopolymerization scheme was conducted using a simple photomask made of black tapes. First, the photomask was placed onto the glass capillary tube containing the RM mixture with 8CB, followed by UV irradiation at 40 mW/cm^{-2} with a total dosage of 8.0 J/cm^2 (Figure 5a). Then, the opposite side of the tube was irradiated at the same intensity by placing the photomask onto exactly the opposite side of the exposed regions in the first step; one edge of the tube was completely blocked by the black tape during both UV irradiations. Last, the unexposed edge was UV cured at 70 mW/cm^{-2} of the same dosage as the other two UV irradiations. After removal of 8CB with ethanol, followed by

https://doi.org/10.1021/acsami.2c14947
ACS Appl. Mater. Interfaces 2022, 14, 50171−50179

drying, a flower-shaped H-LCN filament was formed, as the result of alternating positive and negative curvatures generated in the UV-exposed outer surface and porous inner surface (Figure 5b,c and Movie S2). When immersed in chloroform, the flower-shaped filament was straightened; the whole process was reversible (Movie S2). In a similar manner, a single filament can be effectively programmed with different curvatures and bending directions (Figure 5d), producing, e.g., the letters UPENN (Figure 5e).

As mentioned before, filaments are of interest in applications such as artificial muscles,[5,22] smart fabrics,[7] and soft robots.[6] Since our filament has a cylindrical geometry, we can control the direction of bending by UV-irradiation in different radial angles (Figure 5f). Similar to the UV-polymerization process reported earlier, first a black tape photomask was placed onto the both edges of the capillary tube and irradiated with UV light at an intensity of 30 mW/cm^{-2}. In the second step, the capillary tube was rotated by 90° and the remaining unpolymerized mixture was irradiated in the middle by UV light at 45.6 mW/cm^{-2}. After removal of 8CB and being dried, the filament started to fold into a hook with different angles of bending (Figure 5g,h and Movie S3). In contrast, P-LCN filaments prepared in the same manner, whether for flowerlike or hooklike folded structures, only showed irregularly folded patterns even though the filaments follow the same sequence of folding as H-LCN filaments (Figure S6).

Finally, to utilize the glassy, fold filaments, e.g., the hook seen in Figure 5g to do work, we first characterized the mechanical properties of the H-LCN filament which was prepared with UV light at 76.0 mW/cm^{-2}; thus, it shows a straight filament. The tensile stress−strain curves of the dried and swollen H-LCN filament are presented in Figure 5i, which can be elongated by 8 and 12%, respectively. Due to the densely crosslinked network architecture, the dried H-LCN is much harder and more brittle (E ∼ 650 MPa) than a conventional LCE (E in the order of a few MPa).[66,67] When the LCN is fully swollen in chloroform, E decreased to ∼1 MPa. The large change of moduli in the dry vs the wet state is similar to or even larger than that of many thermoplastics near T_g, from 0.01 to 3 GPa.[68] Such a large modulus change can be utilized for tunable stiffness in soft robotics, e.g., gripping and release of an object. Here, we used the H-LCN filament to wrap an object by designing the bending actuation at the designated sites. When the swollen H-LCN filament was placed onto a bolt, the filament could compliantly contact the bolt and then gradually grab it in the order of seconds during solvent evaporation (Movie S4). When it is immersed in chloroform, the filament could release the bolt. To estimate the pulling force the gripper could generate, we installed the gripper in a tensile machine to pull the subject fixed on the bottom vertically (Figure 5j). The pulling force rapidly increased at the initial stage (Figure 5j, first inset). Then, the filament started to slip on the gripped object, leading to saturation of the pulling force (Figure 5j, second inset). Finally, the gripper was completely separated from the gripped object (Figure 5j, third inset). The maximum force this gripper can generate is 0.35 N, which is more than 7000 times its own weight, ∼50 μN.

4. CONCLUSIONS

In summary, for the first time, self-folding LCN filaments with homeotropic alignment of mesogens are demonstrated, presenting bending-dominant deformation. Unlike typical methods to produce filaments based on extrusion, where mesogens are aligned along the filament long axis, here, we realize vertical alignment of mesogens relative to the long axis of the filament by controlling the anchoring condition of the inner surface of a cylindrical glass tube. Compared with LCN filaments with planar oriented mesogens where both bending and twisting could occur and compete with each other upon swelling, filaments with vertical mesogen alignment undergo bending dominant deformation, which maximizes the directional expansion and contraction in-between polymeric chains, thus offering better control of shape changes. The degree of alignment can be tuned by the concentration of smectic-phase nonreactive mesogens in the reactive mixtures. By varying UV intensity, we can control the LCN crosslinking density gradient through the filament thickness and/or laterally via sequential photocrosslinking using photomasks, forming asymmetric porous structures in different locations and directions, thus offering local control of the degrees of bending for complex 3D shapes. Finally, the dramatic switching from the rigid glassy LCN to a soft swollen LCE allows us to create a highly efficient gripper that can reversible grip and release an object. Our approach offers new insights to engineer and manipulate polymeric filaments for soft robotics or smart fabrics.

■ ASSOCIATED CONTENT

Supporting Information

The Supporting Information is available free of charge at https://pubs.acs.org/doi/10.1021/acsami.2c14947.

Illustration of the experimental process, DSC thermograms, SEM images, and FT-IR spectra (PDF)

Solvent-swelling and deswelling actuation of H-LCP and P-LCN filaments (MP4)

Solvent-swelling and deswelling actuation of flower like H-LCN filaments (MP4)

Solvent-swelling and deswelling actuation of 3D H-LCN filament (MP4)

H-LCN grapping and releasing a bolt (MP4)

■ AUTHOR INFORMATION

Corresponding Author

Shu Yang − *Department of Materials Science and Engineering, University of Pennsylvania, Philadelphia, Pennsylvania 19104, United States;* orcid.org/0000-0001-8834-3320; Email: shuyang@seas.upenn.edu

Authors

Dae Seok Kim − *Department of Materials Science and Engineering, University of Pennsylvania, Philadelphia, Pennsylvania 19104, United States; Department of Polymer Engineering, Pukyong National University, Busan 48513, South Korea*

Young-Joo Lee − *Department of Materials Science and Engineering, University of Pennsylvania, Philadelphia, Pennsylvania 19104, United States*

Yuchen Wang − *Department of Materials Science and Engineering, University of Pennsylvania, Philadelphia, Pennsylvania 19104, United States;* orcid.org/0000-0002-6710-6710

Jinseok Park − *Department of Materials Science and Engineering, University of Pennsylvania, Philadelphia, Pennsylvania 19104, United States*

https://doi.org/10.1021/acsami.2c14947
ACS Appl. Mater. Interfaces 2022, 14, 50171−50179

Karen I. Winey − *Department of Materials Science and Engineering, University of Pennsylvania, Philadelphia, Pennsylvania 19104, United States;* orcid.org/0000-0001-5856-3410

Complete contact information is available at: https://pubs.acs.org/10.1021/acsami.2c14947

Author Contributions

D.S.K. and S.Y. conceived the research ideas; D.S.K. developed and prepared materials; D.S.K. conducted optical characterization; D.S.K. and Y.-J.L. conducted the mechanical characterization; Y.W. conducted the thermal characterization; D.S.K., J.P., and K.I. Winey. conducted X-ray diffraction characterization; D.S.K., Y.-J.L., Y.W., J.P., and S.Y. wrote the manuscript; S.Y. supervised the research. All authors read and commented on the manuscript.

Notes

The authors declare no competing financial interest.

■ ACKNOWLEDGMENTS

We acknowledge support by National Science Foundation (NSF) through Materials Research Science and Engineering Center at University of Pennsylvania, DMR-1720530, and NSF/DMR-POLY program, DMR-2104841 (S.Y.), and by the National Research Foundation of Korea (NRF) grant funded by the Korea government (MSIT), 2021R1F1A1047516 (D.S.K.).

■ REFERENCES

(1) Majidi, C. Soft-Matter Engineering for Soft Robotics. *Adv. Mater. Technol.* **2018**, No. 1800477.
(2) Fan, J.; He, Q.; Liu, Y.; Zhang, F.; Yang, X.; Wang, Z.; Lu, N.; Fan, W.; Lin, L.; Niu, G.; He, N.; Song, J.; Chen, X. Light-Responsive Biodegradable Nanomedicine Overcomes Multidrug Resistance via NO-Enhanced Chemosensitization. *ACS Appl. Mater. Interfaces* **2016**, *8*, 13804−13811.
(3) Cui, H.; Hensleigh, R.; Yao, D.; Maurya, D.; Kumar, P.; Kang, M. G.; Priya, S.; Zheng, X. Three-Dimensional Printing of Piezoelectric Materials with Designed Anisotropy and Directional Response. *Nat. Mater.* **2019**, *18*, 234−241.
(4) Kim, J.; Kim, J. W.; Kim, H. C.; Zhai, L.; Ko, H.-U.; Muthoka, R. M. Review of Soft Actuator Materials. *Int. J. Precis. Eng. Manuf.* **2019**, *20*, 2221−2241.
(5) Wang, J.; Gao, D.; Lee, P. S. Recent Progress in Artificial Muscles for Interactive Soft Robotics. *Adv. Mater.* **2021**, *33*, No. 2003088.
(6) Palagi, S.; Fischer, P. Bioinspired Microrobots. *Nat. Rev. Mater.* **2018**, *3*, 113−124.
(7) Smith, M. K.; Mirica, K. A. Self-Organized Frameworks on Textiles (SOFT): Conductive Fabrics for Simultaneous Sensing, Capture, and Filtration of Gases. *J. Am. Chem. Soc.* **2017**, *139*, 16759−16767.
(8) Ware, T. H.; McConney, M. E.; Wie, J. J.; Tondiglia, V. P.; White, T. J. Voxelated Liquid Crystal Elastomers. *Science* **2015**, *347*, 982−984.
(9) Aharoni, H.; Xia, Y.; Zhang, X.; Kamien, R. D.; Yang, S. Universal Inverse Design of Surfaces with Thin Nematic Elastomer Sheets. *Proc. Natl. Acad. Sci. U. S. A.* **2018**, *115*, 7206−7211.
(10) Liu, J.; Gao, Y.; Lee, Y.-J.; Yang, S. Responsive and Foldable Soft Materials. *Trends Chem.* **2020**, *2*, 107−122.
(11) Jeon, S.-J.; Hauser, A. W.; Hayward, R. C. Shape-Morphing Materials from Stimuli-Responsive Hydrogel Hybrids. *Acc. Chem. Res.* **2017**, *50*, 161−169.
(12) Besse, N.; Rosset, S.; Zarate, J. J.; Shea, H. Flexible Active Skin: Large Reconfigurable Arrays of Individually Addressed Shape Memory Polymer Actuators. *Adv. Mater. Technol.* **2017**, *2*, No. 1700102.
(13) White, T. J.; Broer, D. J. Programmable and Adaptive Mechanics with Liquid Crystal Polymer Networks and Elastomers. *Nat. Mater.* **2015**, *14*, 1087−1098.
(14) Gu, G.-Y.; Zhu, J.; Zhu, L.-M.; Zhu, X. A Survey on Dielectric Elastomer Actuators for Soft Robots. *Bioinspiration Biomimetics* **2017**, *12*, No. 011003.
(15) Martinez, R. V.; Fish, C. R.; Chen, X.; Whitesides, G. M. Elastomeric Origami: Programmable Paper-Elastomer Composites as Pneumatic Actuators. *Adv. Funct. Mater.* **2012**, *22*, 1376−1384.
(16) Küpfer, J.; Finkelmann, H. Nematic liquid single crystal elastomers. *Makromol. Chem., Rapid Commun.* **1991**, *12*, 717−726.
(17) Boothby, J. M.; Kim, H.; Ware, T. H. Shape Changes in Chemoresponsive Liquid Crystal Elastomers. *Sens. Actuators, B* **2017**, *240*, 511−518.
(18) Harris, K. D.; Bastiaansen, C. W. M.; Broer, D. J. A Glassy Bending-Mode Polymeric Actuator Which Deforms in Response to Solvent Polarity. *Macromol. Rapid Commun.* **2006**, *27*, 1323−1329.
(19) Lee, K. M.; Tabiryan, N. V.; Bunning, T. J.; White, T. J. Photomechanical Mechanism and Structure-Property Considerations in the Generation of Photomechanical Work in Glassy, Azobenzene Liquid Crystal Polymer Networks. *J. Mater. Chem.* **2012**, *22*, 691−698.
(20) You, R.; Kang, S.; Lee, C.; Jeon, J.; Wie, J. J.; Kim, T.-S.; Yoon, D. K. Programmable Liquid Crystal Defect Arrays via Electric Field Modulation for Mechanically Functional Liquid Crystal Networks. *ACS Appl. Mater. Interfaces* **2021**, *13*, 36253−36261.
(21) Hu, Z.; Li, Y.; Lv, J. Phototunable Self-Oscillating System Driven by a Self-Winding Fiber Actuator. *Nat. Commun.* **2021**, *12*, 3211.
(22) Mu, J.; Jung de Andrade, M.; Fang, S.; Wang, X.; Gao, E.; Li, N.; Kim, S. H.; Wang, H.; Hou, C.; Zhang, Q.; Zhu, M.; Qian, D.; Lu, H.; Kongahage, D.; Talebian, S.; Foroughi, J.; Spinks, G.; Kim, H.; Ware, T. H.; Sim, H. J.; Lee, D. Y.; Jang, Y.; Kim, S. J.; Baughman, R. H. Sheath-Run Artificial Muscles. *Science* **2019**, *365*, 150−155.
(23) Chu, H.; Hu, X.; Wang, Z.; Mu, J.; Li, N.; Zhou, X.; Fang, S.; Haines, C. S.; Park, J. W.; Qin, S.; Yuan, N.; Xu, J.; Tawfick, S.; Kim, H.; Conlin, P.; Cho, M.; Cho, K.; Oh, J.; Nielsen, S.; Alberto, K. A.; Razal, J. M.; Foroughi, J.; Spinks, G. M.; Kim, S. J.; Ding, J.; Leng, J.; Baughman, R. H. Unipolar Stroke, Electroosmotic Pump Carbon Nanotube Yarn Muscles. *Science* **2021**, *371*, 494−498.
(24) Liu, J.; Gao, Y.; Wang, H.; Poling-Skutvik, R.; Osuji, C. O.; Yang, S. Shaping and Locomotion of Soft Robots Using Filament Actuators Made from Liquid Crystal Elastomer−Carbon Nanotube Composites. *Adv. Intell. Syst.* **2020**, *2*, No. 1900163.
(25) Pilz da Cunha, M.; Ambergen, S.; Debije, M. G.; Homburg, E. F. G. A.; den Toonder, J. M. J.; Schenning, A. P. H. J. A Soft Transporter Robot Fueled by Light. *Adv. Sci.* **2020**, *7*, No. 1902842.
(26) Kuenstler, A. S.; Kim, H.; Hayward, R. C. Liquid Crystal Elastomer Waveguide Actuators. *Adv. Mater.* **2019**, *31*, No. 1901216.
(27) Lv, J.; Liu, Y.; Wei, J.; Chen, E.; Qin, L.; Yu, Y. Photocontrol of Fluid Slugs in Liquid Crystal Polymer Microactuators. *Nature* **2016**, *537*, 179−184.
(28) Zmyślony, M.; Dradrach, K.; Haberko, J.; Nałęcz-Jawecki, P.; Rogóż, M.; Wasylczyk, P. Optical Pliers: Micrometer-Scale, Light-Driven Tools Grown on Optical Fibers. *Adv. Mater.* **2020**, *32*, No. 2002779.
(29) Kuang, X.; Roach, D. J.; Wu, J.; Hamel, C. M.; Ding, Z.; Wang, T.; Dunn, M. L.; Qi, H. J. Advances in 4D Printing: Materials and Applications. *Adv. Funct. Mater.* **2019**, *29*, No. 1805290.
(30) Krause, S.; Dersch, R.; Wendorff, J. H.; Finkelmann, H. Photocrosslinkable Liquid Crystal Main-Chain Polymers: Thin Films and Electrospinning. *Macromol. Rapid Commun.* **2007**, *28*, 2062−2068.
(31) Sharma, A.; Lagerwall, J. Electrospun Composite Liquid Crystal Elastomer Fibers. *Materials* **2018**, *11*, 393.

(32) Lu, M.; Sharifi, F.; Hashemi, N. N.; Montazami, R. Fluid-Induced Alignment of Carbon Nanofibers in Polymer Fibers. *Macromol. Mater. Eng.* **2017**, *302*, No. 1600544.
(33) Lin, X.; Saed, M. O.; Terentjev, E. M. Continuous Spinning Aligned Liquid Crystal Elastomer Fibers with a 3D Printer Setup. *Soft Matter* **2021**, *17*, 5436−5443.
(34) Verpaalen, R. C. P.; Pilz da Cunha, M.; Engels, T. A. P.; Debije, M. G.; Schenning, A. P. H. J. Liquid Crystal Networks on Thermoplastics: Reprogrammable Photo-Responsive Actuators. *Angew. Chem., Int. Ed.* **2020**, *59*, 4532−4536.
(35) Dong, L.; Tong, X.; Zhang, H.; Chen, M.; Zhao, Y. Near-Infrared Light-Driven Locomotion of a Liquid Crystal Polymer Trilayer Actuator. *Mater. Chem. Front.* **2018**, *2*, 1383−1388.
(36) Gerbode, S. J.; Puzey, J. R.; McCormick, A. G.; Mahadevan, L. How the Cucumber Tendril Coils and Overwinds. *Science* **2012**, *337*, 1087−1091.
(37) van Oosten, C. L.; Bastiaansen, C. W. M.; Broer, D. J. Printed Artificial Cilia from Liquid-Crystal Network Actuators Modularly Driven by Light. *Nat. Mater.* **2009**, *8*, 677−682.
(38) Antman, S. S. *Nonlinear Problems of Elasticity*; Springer: New York, 2004.
(39) O'Reilly, O. M. *Modeling Nonlinear Problems in the Mechanics of Strings and Rods: The Role of the Balance Laws*; Springer: New York, N18, 2017.
(40) Wu, H.; Zheng, Y.; Zeng, Y. Fabrication of Helical Nanofibers via Co-Electrospinning. *Ind. Eng. Chem. Res.* **2015**, *54*, 987−993.
(41) Liu, J.; Huang, J.; Su, T.; Bertoldi, K.; Clarke, D. R. Structural Transition from Helices to Hemihelices. *PLoS One* **2014**, *9*, No. e93183.
(42) Sawa, Y.; Urayama, K.; Takigawa, T.; Gimenez-Pinto, V.; Mbanga, B. L.; Ye, F.; Selinger, J. V.; Selinger, R. L. B. Shape and Chirality Transitions in Off-Axis Twist Nematic Elastomer Ribbons. *Phys. Rev. E: Stat., Nonlinear, Soft Matter Phys.* **2013**, *88*, No. 022502.
(43) Iamsaard, S.; Aßhoff, S. J.; Matt, B.; Kudernac, T.; Cornelissen, J. J. L. M.; Fletcher, S. P.; Katsonis, N. Conversion of Light into Macroscopic Helical Motion. *Nat. Chem.* **2014**, *6*, 229−235.
(44) Wang, M.; Lin, B.-P.; Yang, H. A Plant Tendril Mimic Soft Actuator with Phototunable Bending and Chiral Twisting Motion Modes. *Nat. Commun.* **2016**, *7*, 13981.
(45) Studart, A. R.; Erb, R. M. Bioinspired Materials That Self-Shape through Programmed Microstructures. *Soft Matter* **2014**, *10*, 1284−1294.
(46) Yamaoka, H.; Adachi, T. Coupling between Axial Stretch and Bending/Twisting Deformation of Actin Filaments Caused by a Mismatched Centroid from the Center Axis. *Int. J. Mech. Sci.* **2010**, *52*, 329−333.
(47) de Haan, L. T.; Verjans, J. M. N.; Broer, D. J.; Bastiaansen, C. W. M.; Schenning, A. P. H. J. Humidity-Responsive Liquid Crystalline Polymer Actuators with an Asymmetry in the Molecular Trigger That Bend, Fold, and Curl. *J. Am. Chem. Soc.* **2014**, *136*, 10585−10588.
(48) Lee, W.-E.; Jin, Y.-J.; Park, L.-S.; Kwak, G. Fluorescent Actuator Based on Microporous Conjugated Polymer with Intramolecular Stack Structure. *Adv. Mater.* **2012**, *24*, 5604−5609.
(49) Hikmet, R. A. M. Anisotropic Gels and Plasticized Networks Formed by Liquid Crystal Molecules. *Liq. Cryst.* **1991**, *9*, 405−416.
(50) Hikmet, R. A. M. Anisotropic Gels in Liquid Crystal Devices. *Adv. Mater.* **1992**, *4*, 679−683.
(51) Kim, S.-U.; Lee, Y.-J.; Liu, J.; Kim, D. S.; Wang, H.; Yang, S. Broadband and pixelated camouflage in inflating chiral nematic liquid crystalline elastomers. *Nat. Mater.* **2022**, *21*, 41−46.
(52) Kamal, T.; Park, S. Shape-Responsive Actuator from a Single Layer of a Liquid-Crystal Polymer. *ACS Appl. Mater. Interfaces* **2014**, *6*, 18048−18054.
(53) Han, W. C.; Sim, G. W.; Kim, Y. B.; Kim, D. S. Reversible Curvature Reversal of Monolithic Liquid Crystal Elastomer Film and Its Smart Valve Application. *Macromol. Rapid Commun.* **2021**, *42*, No. 2100404.
(54) Yang, D.-K.; Cui, Y.; Nemati, H.; Zhou, X.; Moheghi, A. Modeling Aligning Effect of Polymer Network in Polymer Stabilized Nematic Liquid Crystals. *J. Appl. Phys.* **2013**, *114*, 243515.
(55) Rasing, T.; Muševič, I. *Surfaces and Interfaces of Liquid Crystals*; Springer Berlin Heidelberg: Berlin, Heidelberg, 2004.
(56) Xia, Y.; DeBenedictis, A. A.; Kim, D. S.; Chen, S.; Kim, S.-U.; Cleaver, D. J.; Atherton, T. J.; Yang, S. Programming Emergent Symmetries with Saddle-Splay Elasticity. *Nat. Commun.* **2019**, *10*, 5104.
(57) Joralmon, D.; Alfarhan, S.; Kim, S.; Tang, T.; Jin, K.; Li, X. Three-Dimensional Printing of Liquid Crystals with Thermal Sensing Capability via Multimaterial Vat Photopolymerization. *ACS Appl. Polym. Mater.* **2022**, *4*, 2951−2959.
(58) Karausta, A.; Bukusoglu, E. Liquid Crystal-Templated Synthesis of Mesoporous Membranes with Predetermined Pore Alignment. *ACS Appl. Mater. Interfaces* **2018**, *10*, 33484−33492.
(59) Zhan, X.; Luo, D.; Yang, K.-L. Multifunctional sensors based on liquid crystals scaffolded in nematic polymer networks. *RSC Adv.* **2021**, *11*, 38694−38702.
(60) Leonzio, G. Methanol Synthesis: Optimal Solution for a Better Efficiency of the Process. *Processes* **2018**, *6*, 20.
(61) Kleman, M., Lavrentovich, O. D. *Soft Matter Physics: An Introduction*; Springer: New York, 2003.
(62) Toquer, G.; Phou, T.; Monge, S.; Grimaldi, A.; Nobili, M.; Blanc, C. Colloidal Shape Controlled by Molecular Adsorption at Liquid Crystal Interfaces. *J. Phys. Chem. B* **2008**, *112*, 4157−4160.
(63) Jerome, B. Surface Effects and Anchoring in Liquid Crystals. *Rep. Prog. Phys.* **1991**, *54*, 391−451.
(64) Noh, J.; Henx, B.; Lagerwall, J. P. F. Taming Liquid Crystal Self-Assembly: The Multifaceted Response of Nematic and Smectic Shells to Polymerization. *Adv. Mater.* **2016**, *28*, 10170−10174.
(65) Stapert, H. R.; del Valle, S.; Verstegen, E. J. K.; van der Zande, B. M. I.; Lub, J.; Stallinga, S. Photoreplicated Anisotropic Liquid-Crystalline Lenses for Aberration Control and Dual-Layer Readout of Optical Discs. *Adv. Funct. Mater.* **2003**, *13*, 732−738.
(66) Wang, Y.; Liu, J.; Yang, S. Multi-Functional Liquid Crystal Elastomer Composites. *Appl. Phys. Rev.* **2022**, *9*, No. 011301.
(67) Xia, Y.; Zhang, X.; Yang, S. Instant Locking of Molecular Ordering in Liquid Crystal Elastomers by Oxygen-Mediated Thiol−Acrylate Click Reactions. *Angew. Chem., Int. Ed.* **2018**, *57*, 5665−5668.
(68) Wang, L.; Yang, Y.; Chen, Y.; Majidi, C.; Iida, F.; Askounis, E.; Pei, Q. Controllable and Reversible Tuning of Material Rigidity for Robot Applications. *Mater. Today* **2018**, *21*, 563−576.

https://doi.org/10.1021/acsami.2c14947
ACS Appl. Mater. Interfaces 2022, 14, 50171−50179